ISSN: 2688-8645

Numerical Simulation Study of Droplet Atomization Behavior in Tubular Atomizer Elements

Zhenqiang Kang, Liang Zhang *, Xin Chen

School of Mechatronic Engineering, Southwest Petroleum University, Chengdu, Sichuan, China

* Corresponding author: Liang Zhang

Abstract

Atomizing a liquid solvent into micron-sized droplets can significantly increase the specific contact area between the gas phase and the liquid phase. This paper employs CFD methods to investigate the atomization performance of a tubular natural gas atomizer and analyzes the effects of four different gas flow velocities (18 m/s–23 m/s) on the atomization efficiency. The results indicate that the use of a Venturi channel structure, where peak gas velocities in the throat region exceed 90–110 m/s, effectively breaks the liquid into small droplets. In the high-frequency pulsation transition zone at 18 m/s and 23 m/s, irregular turbulent diffusion enhances interphase mixing, rapidly entraining fragmented microdroplets of triethylene glycol into every corner of the gas phase, thereby significantly reducing concentration polarization within the flow field. The wake effect generated by the hollow channel results in a higher DPM concentration in the region around the central axis. A comparative analysis of the four velocities revealed that 18 m/s is more suitable for droplet atomization.

Keywords

Liquid Jet; Droplet Breakup; Droplet Size.

1. Introduction

Atomizing a liquid solvent into micron-sized droplets significantly increases the specific contact area between the gas and liquid phases. The excellent tracking behavior of micron-sized droplets in a gas stream also facilitates uniform dispersion and mixing between the gas and liquid phases, thereby enhancing gas-liquid mass transfer processes in the energy and chemical industries. The droplet distribution and gas-liquid mass transfer characteristics of Venturi scrubbers and spray towers have been extensively studied, with a focus on enhancing gas-liquid mass transfer through the atomization of absorbents[1-4]. This technology holds broad application prospects in the energy and chemical industries. A common feature of these compact and efficient tubular gas-liquid contactors is that liquid is injected into a high-velocity gas stream through nozzles uniformly distributed within the tubular space; the liquid stream is subjected to shear forces within the gas stream, breaking it into micron-sized droplets with small diameters and a uniform particle size distribution. These micron-sized droplets disperse within intense turbulence and come into contact with the gas, thereby enhancing gas-liquid mixing and mass transfer efficiency. The key to effective gas-liquid atomization and mixing lies in the effective utilization of the liquid phase, while the mixing efficiency also depends on the dispersion space of the droplets within the tube and the gas flow conditions.

The initial breakup of a liquid jet is one of the fundamental processes in atomization. Current research focuses primarily on characteristics such as the breakup patterns and penetration depth of liquid jets. Within a tube, the liquid jet bends under the influence of aerodynamic forces, generating surface waves[5]. Changes in the jet's shape affect the forces acting on its surface, and both the forces and the shape undergo frequent fluctuations. When the forces acting on the

ISSN: 2688-8645

jet momentarily become unbalanced at a given instant, the jet randomly breaks up into droplets of varying sizes. Wu[6] discussed the wavelength of surface waves propagating along a liquid column, the deformation of the liquid column prior to rupture at the liquid surface, and the conditions under which droplets begin to form on the liquid surface; he also analyzed the effect of the liquid column jet velocity on the penetration depth of the jet. Oda et al.[7] investigated jet penetration, jet width, and spray characteristics in subsonic cross-flow. In subsonic lateral flow, the mechanisms governing droplet formation differ between the near-field and far-field regions of the liquid column. During the breakup of the liquid column, the formation of liquid clumps and droplets is primarily driven by the breakup of the liquid column itself and surface wave breakup, whereas the formation of fine droplets is mainly driven by surface wave breakup of the liquid column[8-9]. Lubarsky et al. [10] found that, in the direction of the transverse airflow—particularly in the core region of the spray—there is a significant lag between the droplet velocity and the average velocity of the incoming airflow. Existing research indicates that the spray characteristics of liquid flows in lateral air currents are primarily influenced by the gas-liquid velocity ratio, the Weber number, and specific parameters of the air flow. However, diagrams of liquid jet breakup patterns, empirical formulas for jet trajectories, and droplet size prediction formulas are only applicable under specific experimental conditions; therefore, their results are not universally applicable. Furthermore, the aforementioned studies have primarily focused on the liquid jet breakup process in uniform gas flows, while research on the mechanisms of liquid jet breakup in non-uniform gas flows remains limited.

Based on gas-liquid atomization theory, the basic structure of a tubular gas-liquid atomization mixer was proposed. Computational fluid dynamics (CFD) numerical simulation techniques were used to analyze the droplet size and velocity distributions at the outlet of the atomization element in a tubular natural gas dehydration unit, as well as the velocity and turbulence intensity distributions of the gas flow within the flow channel. The results of this study can serve as a foundation for the design of atomizing elements in tubular natural gas dehydration equipment and provide theoretical guidance and data support for the optimization of tubular atomizing mixers.

2. Numerical Simulation Methods

2.1. Geometry and Mesh Generation of Atomization Elements

2.1.1. Geometry of Atomization Elements

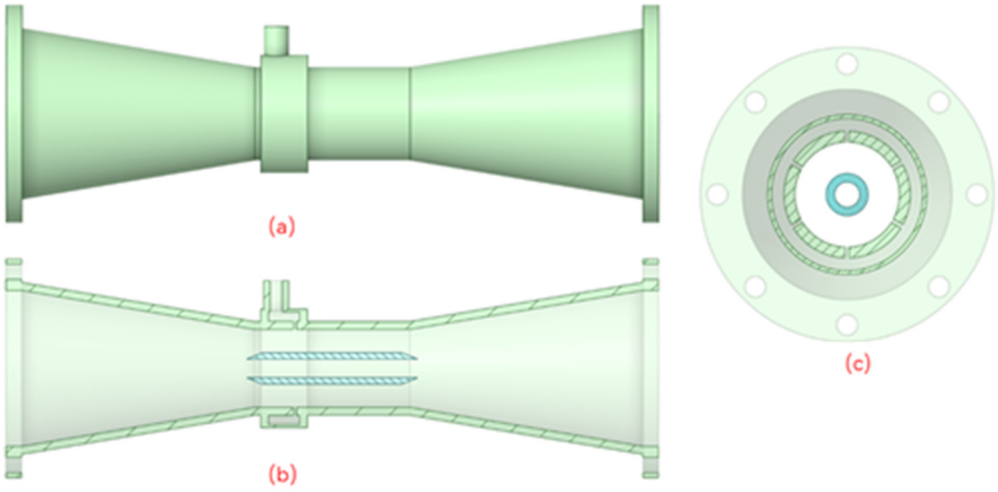

Fig 1. Geometric Model of the Atomization Element, Fig.1(a) shows the complete geometry; (b) shows the XY cross-section; (c) shows the distribution of the nozzle inlets.

ISSN: 2688-8645

The tubular natural gas atomization device primarily consists of a Venturi flow channel and six nozzle inlets, as shown in Fig.1. Figure (a) depicts the complete geometric structure, with an overall length of 400 mm, D_1 = 100 mm, a throat length of 100 mm, and a tube diameter D_2 of 50 mm. As the gas flows through the throat, its velocity increases to nearly four times that at the inlet. The Venturi channel is divided into a converging section, a throat, and a diverging section. The angles between the converging and diverging sections and the channel centerline are less than 15°, meeting the design requirements for Venturi channels. A hollow flow-guiding structure is positioned at the center of the Venturi flow channel to provide a high-velocity gas stream to the downstream channel, preventing droplet coalescence at the entrance to the expansion section. Six nozzles are evenly distributed in the radial region of the throat, as shown in Fig.1(c). The nozzle diameter is φ = 2 mm, and an annular liquid flow channel is arranged around the exterior of the nozzle to provide a continuous liquid supply.

2.1.2. Mesh Generation of Atomization Elements

To balance the fit of complex geometric configurations with computational convergence, this study employs a hybrid meshing strategy combining unstructured tetrahedral meshes with boundary layer polyhedral meshes. The overall mesh is shown in Fig. 2. In regions where the fluid exhibits significant normal velocity gradients, such as on wall surfaces and the surfaces of hollow flow-guiding structures, a five-layer boundary layer mesh was generated. By controlling the height of the first layer (y+ ≈ 1), the mesh satisfies the requirements of the turbulence model for solving the viscous sublayer near the wall. At the same time, to accurately capture the fragmentation behavior of triethylene glycol under high-speed natural gas shear after it is sprayed from the six inlet holes, local mesh refinement was performed on the triethylene glycol annular flow channel, the high-shear zone at the throat, and the wake evolution zone at the trailing edge of the hollow flow-guiding structure.

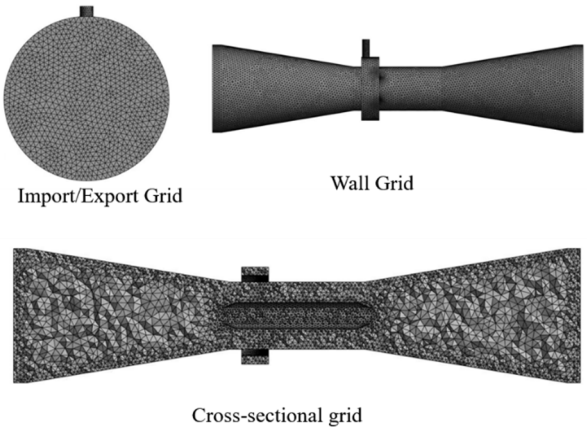

Fig 2. Grid Division

2.2. Verification of Mesh Independence.

In this study, while maintaining consistency in the overall topological structure and boundary layer parameters, four mesh models with varying numbers of elements were generated by adjusting the overall global dimensions and local refinement levels. The number of elements was approximately 850,000 (Mesh 1, coarse), 1,520,000 (Mesh 2, medium), 2,840,000 (Mesh 3, fine), and 4,560,000 (Mesh 4, very fine). The pressure drop (ΔP) at the inlet and outlet and the droplet Saltzman mean diameter (SMD) at the outlet of the gas-aerosol mixer were selected as metrics for evaluating grid independence. The inlet and outlet pressure drop reflects the computational accuracy of the grid resolution regarding frictional resistance losses along the pipeline and the throttling effects of the contraction and expansion sections, while the droplet Saltzman mean diameter at the outlet of the gas-aerosol mixer directly verifies the grid's ability to capture the airflow shear layer and droplet secondary fragmentation behavior.

ISSN: 2688-8645

As shown as Fig. 3, when the number of grid cells increased from 1.52 million (Grid 2) to 2.84 million (Grid 3), the flow field shear layer was fully resolved, the droplet atomization model gradually became effective, and all monitored data began to show a significant convergence trend. Furthermore, when the number of mesh cells was further increased from 2.84 million to 4.56 million (Mesh 4), not only did the difference in macroscopic pressure drop converge to within 0.5%, but even the relative error in droplet diameter—a parameter highly sensitive to mesh resolution—was effectively controlled below 0.93%, remaining within the permissible error range for engineering numerical simulations (typically <5%). Taking into account the accuracy of numerical calculations and computational efficiency, while balancing hardware computing power, all subsequent studies of varying operating conditions and flow field characteristic analyses in this paper were performed using a mesh architecture with the same mesh scale and partitioning strategy as Mesh 3 (2,841,533 cells).

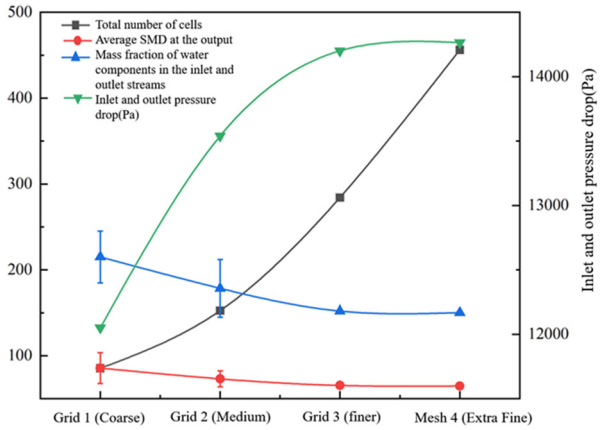

Fig 3. Verification of grid independence

2.3. Boundary Condition Settings

Four velocity gradients as 10 m/s, 15 m/s, 18 m/s, and 23 m/s were set as comparison conditions. The inlet operating pressure was set to 5 MPa, and the pressure input at all boundaries was gauge pressure. The turbulence intensity was set to 5%, and the hydraulic diameter was determined based on the inlet pipe diameter D=100 mm. The outlet gauge pressure is set to 0 Pa, meaning the outlet end maintains an absolute pressure environment of 5 MPa. The turbulence intensity is also set to 5% to prevent numerical backflow at the outlet—which could lead to computational divergence—under conditions of large flow fluctuations. Both the flow channel walls and the surface of the hollow flow guide are defined as non-slip, adiabatic, rigid walls. The boundary condition for the wall relative to the discrete phase particles is set to “Reflect” to simulate the reflection of droplets off the wall.

3. Results and Discussion

3.1. Patterns of Flow Velocity Distribution in Atomization Elements

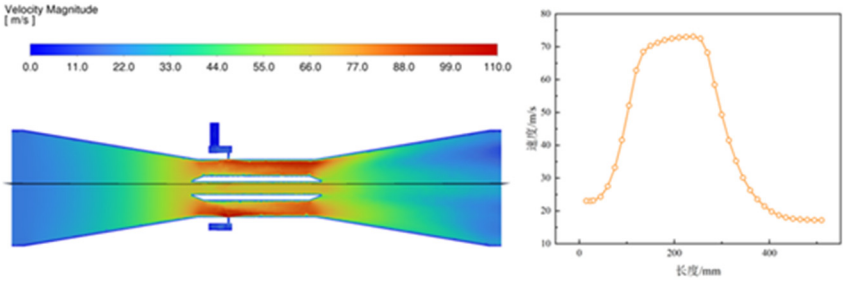

Fig 4. Velocity contour plot and axial velocity when v = 18 m/s

ISSN: 2688-8645

Fig. 4 shows a velocity distribution contour plot of the XY cross-section of the atomizing element. As can be seen from the figure, the flow patterns within the atomizing element exhibit a high degree of geometric dependence. The entire flow field can be divided into three distinct regions: the converging acceleration section of the Venturi structure, the throat atomization section, and the diverging pressure-increasing section. After entering through the inlet on the left, the natural gas-water mixture undergoes axial acceleration due to the conical, converging structure of the tube wall. Since the fluid must obey the equations of mass conservation and continuity, it converts static pressure energy into kinetic energy under the physical constraint of a continuously decreasing cross-sectional area of the flow channel. In the converging section of the atomization element, the gas velocity undergoes a smooth transition from low to high speeds. The flow field in this region is relatively clean, dominated by one-dimensional and two-dimensional axisymmetric flow, with a relatively gentle radial distribution of the velocity gradient. The thickness of the boundary layer at the pipe wall gradually decreases in this region, providing a pre-acceleration foundation for the subsequent intense gas-liquid collision in the throat region and ensuring that the gas flow possesses sufficient momentum flux upon reaching the inlet. The throat region is where kinetic energy evolves most dramatically and fluid dynamics are most complex; it is also the critical zone determining the quality of triethylene glycol atomization. The region of maximum velocity is concentrated and confined to the throat region of the atomization element. Here, the flow cross-sectional area is at its minimum within the entire flow channel structure, and the gas velocity gradually increases to the maximum value within the entire flow channel; in some areas, the peak gas velocity even exceeds 90–110 m/s. In the throat region, the six triethylene glycol droplet inlets are precisely positioned at the core of this ultra-high-velocity annular gap. After undergoing more thorough atomization, the triethylene glycol droplets form an aerosol mixture that enters the gradually expanding duct. In the expansion section, significant kinetic energy dissipation and pressure recovery occur. Immediately behind the hollow guide structure, at the entrance to the expansion section, there is a distinct low-velocity region. During the abrupt transition from high to low velocity, the fluid's ability to overcome the reverse pressure gradient decreases, triggering severe boundary layer separation. Consequently, separation vortices and macroscopic recirculation zones inevitably form at the trailing edge of the hollow guide structure. This aerodynamic recirculation phenomenon has a significant impact on the atomization process. On the one hand, it inevitably causes severe energy loss, leading to an increase in system pressure drop; but simultaneously, the resulting wake vortices increase the turbulence intensity of the flow field, acting as aerodynamic agitation. This forces the triethylene glycol droplets, which have just undergone initial fragmentation, to undergo secondary collisions and tumbling within the vortex structures, greatly extending the residence time of both the liquid and gas phases within the confined volume, thereby enhancing the conversion rate of triethylene glycol in capturing water molecules.

3.2. Analysis of Turbulence Characteristics in Atomization Elements

Fig. 5 shows the analysis of turbulent kinetic energy at the throat cross-section of the atomization element. The figure clearly demonstrates that the macroscopic velocity of the gas flow has a highly significant positive effect on the local pulsating kinetic energy at the throat cross-section. Numerically, as the inlet gas velocity increases, the maximum turbulent kinetic energy of the flow field cross-section exhibits a nonlinear, geometric progression. When the gas velocity v = 10 m/s, the maximum turbulent kinetic energy of the cross-section is approximately 3.29×10^2 m^2/s^2. Under these low-velocity conditions, the overall shear stress of the flow field is relatively weak, and the pulsating region at the center of the flow is small and concentrated. At a gas velocity of 15 m/s, the maximum turbulent kinetic energy across the cross-section rises to 4.14×10^2 m^2/s^2, representing an increase of approximately 25.8% compared to the 10 m/s condition. At this point, the pulsations of the airflow begin to intensify, and the turbulent core

ISSN: 2688-8645

shows a clear tendency to expand. When the gas velocity reaches 18 m/s, the maximum turbulent kinetic energy across the cross-section reaches 5.55×10^2 m^2/s^2, representing a 68.7% increase compared to 10 m/s and marking a very significant jump.

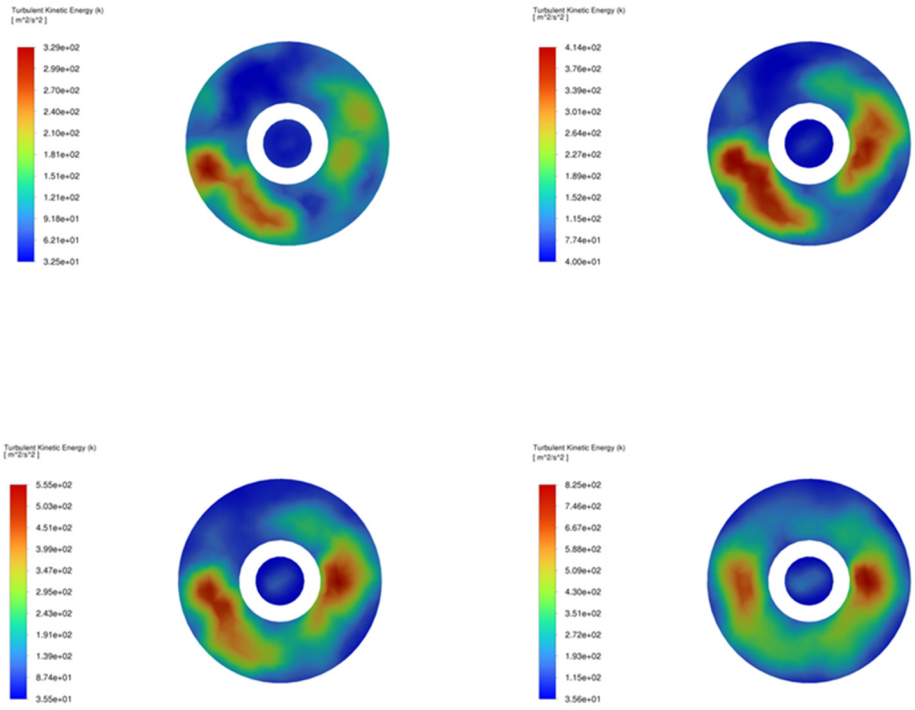

Fig 5. Turbulent kinetic energy in the throat region of an atomizer element at different gas velocities

When the gas velocity reached 23 m/s, the maximum cross-sectional turbulent kinetic energy surged to 8.25×10^2 m^2/s^2, representing the extreme high-velocity condition in this study. The absolute value of the turbulent kinetic energy reached an extremely high level, indicating that gas vortices within the flow field were undergoing extremely intense momentum and energy exchange as well as mutual collisions. Since turbulent kinetic energy is proportional to the square of the fluctuating flow velocity, the shear strain rate caused by internal vortices or structural obstruction increases significantly as the absolute inflow velocity increases. Under the 23 m/s operating condition, two symmetrical regions of strong turbulent kinetic energy on the left and right sides become very distinct with clear boundaries, accompanied by a large transitional zone on the periphery. This indicates that under high-speed conditions, forced convection and vortex shedding dominate, significantly enhancing the penetration capability of the airflow energy across the entire cross-section and effectively improving the velocity non-uniformity of the cross-section. When triethylene glycol (TEG) droplets or liquid films enter these high-energy regions, the massive gas shear stress—driven by the increased inlet gas velocity and the sharp rise in k and ε values—easily overcomes the liquid's surface tension, instantly tearing large droplets into microscopic droplets measuring tens of micrometers. For the high-frequency pulsation transition zones at 18 m/s and 23 m/s, the irregular turbulent diffusion intensifies interphase mixing, rapidly entraining the fragmented micro-TEG droplets into every corner of the gas phase, thereby significantly reducing concentration polarization within the flow field.

3.3. Analysis of the Atomization Performance of Atomization Elements

Fig. 6 shows the atomization performance of the atomizing element at different gas velocities. As can be seen from the figure, as the gas velocity increases, the local peak concentration of

ISSN: 2688-8645

DPM exhibits a significant upward trend: 10.0 kg/m^3 (top left), 12.9 kg/m^3 (top right), 14.4 kg/m^3 (bottom left), and finally surging to a maximum of 16.6 kg/m^3 (bottom right). The continuous rise in the upper limit of the concentration peaks indicates that, during this specific evolutionary process, discrete phase particles undergo a high degree of secondary "compression" and "enrichment" in certain specific regions. In all four images, the red and deep orange patches representing high-concentration enrichment zones consistently cling tightly to the periphery of the outer wall of the central hollow flow guide, as if "attached" to it. Particularly in the cloud plot in the lower right corner (where the maximum reaches 16.6 kg/m^3), the high-concentration core exhibits a distinct asymmetrical protrusion.

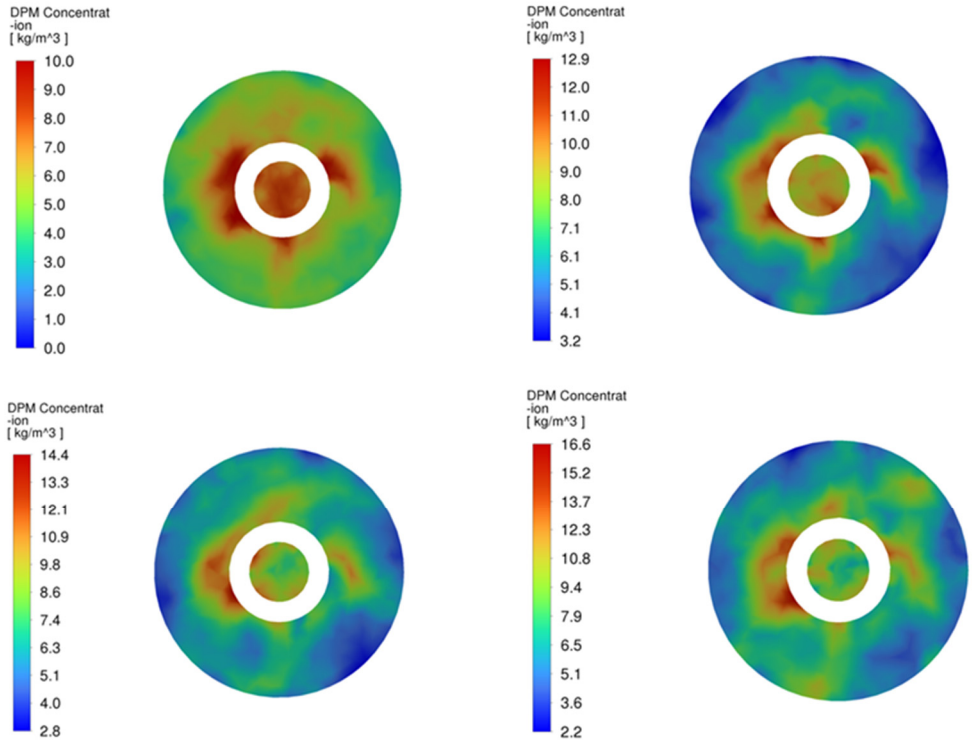

Fig 6. Atomization Performance at the Outlet Interface Under Different Gas Flow Rates

Due to the centrally positioned hollow flow guide structure, the natural gas methane flow inevitably experiences rapid alternations between pressure gradients in the same and opposite directions as it passes the trailing edge, thereby forming a series of detached vortices of varying scales at the trailing edge. These detached vortices possess extremely strong inward negative pressure zones (local low-pressure zones). When triethylene glycol droplets pass through this separation zone with the main flow, the smaller primary atomized droplets—which have excellent followability (low Stokes number)—encounter a sort of "black hole" in the airflow and are forcibly drawn and adsorbed to the area directly behind the flow-guiding device and the near-wall region of the inner ring. This aerodynamic "wake capture" results in a higher DPM concentration in the inner ring.

3.4. Particle Size and Distribution of Aerosol Droplets

As shown in Fig. 7, the particle size frequency distribution curve clearly demonstrates that the atomized droplets at the outlet exhibit nonlinear decay characteristics at different gas velocities. At low gas velocities (10 m/s), the distribution curve exhibits a distinct broad peak, with the peak heavily skewed toward the larger particle size range of 250–300 μm, indicating that the aerodynamic shear energy is far from reaching the break-up threshold of the triethylene glycol solution's surface tension. When the gas velocity enters the optimal range of 18 m/s, the curve

ISSN: 2688-8645

becomes steeper and narrower; this "narrow-peak distribution" indicates a high degree of spray uniformity. However, upon entering the ultra-high gas velocity range of 23 m/s, the curve shifts drastically to the left, with a sharp increase in the proportion of small-diameter droplets (<100 μm). Although this excessive fragmentation increases the specific surface area, the extremely low particle inertia makes them highly prone to being carried directly out with the main gas flow, leading to difficulties in downstream collection.

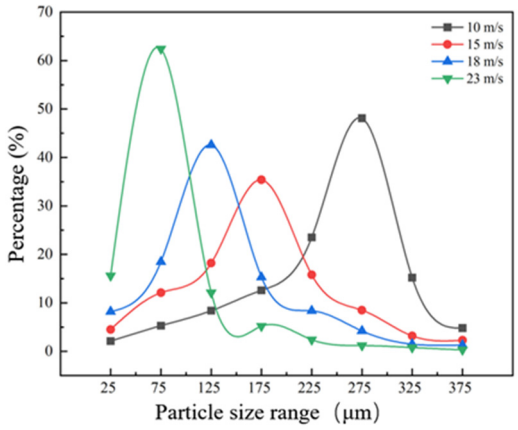

Fig 7. The Effect of Different Gas Velocities on the Droplet Size Distribution at the Atomizer Outlet

As the Weber number (We) increases in accordance with the square law of gas velocity, the SMD drops sharply from 268.4 μm to 81.5 μm. At the same time, the local particle mass concentration shows a clear decreasing trend with increasing gas velocity. This reflects, on the one hand, the high dilution and entrainment capacity of the high-speed gas flow on the liquid phase, and on the other hand, it corroborates the reduced spatial occupancy of the liquid droplet after it is stretched and stripped under high dynamic pressure conditions. The results indicate that around 18 m/s represents the optimal balance between atomization particle size and pressure drop. When the gas velocity was only 10 m/s, the peak of the particle size distribution remained concentrated in the large-scale range of 250–300 μm, accounting for nearly 48%. This was due to the weak relative velocity (difference in momentum flux) between the two phases imparted by the flow field, resulting in a low aerodynamic Reynolds number at the liquid surface. Consequently, the local aerodynamic forces were insufficient to overcome the strong interfacial tension resistance of the triethylene glycol solution itself. As the operating flow velocity increases from 15 m/s to 18 m/s, the peak of the particle size distribution rapidly shifts to the core range of 100–150 μm. At this point, the local Weber number at the gas-liquid jet interface surges dramatically, completely crossing the Rayleigh breakdown region and transitioning to "shear-induced detachment failure," causing the macroscopic liquid flow to be continuously peeled into a fine aerosol. Under the extreme dynamic pressure of 23 m/s, over 60% of the particle diameters decrease to 50–100 μm. At this point, the local particle phase concentration in the cloud image significantly decreases, and the strong entrainment capacity of the high-speed fluid causes the medium to be blown and expanded over long distances.

4. Summary

Based on the above study of tubular natural gas atomization equipment, we can draw the following conclusions:

The throat region is where the kinetic energy of the entire system undergoes the most dramatic changes and where the fluid dynamics are most complex; in some areas, peak gas velocities exceed 90–110 m/s.

ISSN: 2688-8645

In the high-frequency pulsation transition zones at 18 m/s and 23 m/s, the irregular turbulent diffusion enhances interphase mixing, rapidly entraining the fragmented microdroplets of triethylene glycol into every corner of the gas phase, thereby significantly reducing concentration polarization within the flow field.

The wake effect created by the hollow flow channel results in higher DPM concentrations in the area around the central axis.

A comparative analysis of the four speeds was conducted, and 18 m/s was found to be more suitable for droplet atomization.

References

[1] F. Ahmadvand, M.R. Talaie, CFD modeling of droplet dispersion in a Venturi scrubber,Chem. Eng. J. 160 (2) (2010) 423–431 210.

[2] S.W. Lee, H.C. No, Droplet size prediction model based on the upper limit log-normal distribution function in venturi scrubber, Nucl. Eng. Technol. 51 (5) (2019)1261–1271.

[3] M. Ochowiak, L. Broniarz-Press, The flow resistance and aeration in modified spray tower, Chem. Eng. Process. 50 (3) (2011) 345–350.

[4] G. Yincheng, N. Zhenqi, L. Wenyi, Comparison of removal efficiencies of carbon dioxide between aqueous ammonia and NaOH solution in a fine spray column, Energy Procedia 4 (2011) 512–518.

[5] T. Inamura, N. Nagai, Spray characteristics of liquid jet traversing subsonic air-streams, J. Propuls. Power 13 (2) (1997) 250–256.

[6] P.-K. Wu, K.A. Kirkendall, R.P. Fuller, A.S. Nejad, Breakup processes of liquid jets in subsonic crossflows, J. Propuls. Power 13 (1) (1997) 64–73.

[7] T. Oda, H. Hiroyasu, M. Arai, K. Nishida, Characterization of liquid jet atomization across a high-speed airstream, JSME Int. J., Ser. B 37 (4) (1994) 937–944.

[8] M. Broumand, M. Birouk, Liquid jet in a subsonic gaseous crossflow: recent progress and remaining challenges, Prog. Energy Combust. Sci. 57 (2016) 1–29.

[9] M. Behzad, N. Ashgriz, B.W. Karney, Surface breakup of a non-turbulent liquid jet injected into a high pressure gaseous crossflow, Int. J. Multiphase Flow 80 (2016)100–117.

[10] E. Lubarsky, J.R. Reichel, B.T. Zinn, R. McAmis, Spray in crossflow: dependence on weber number, J. Eng. Gas Turbines Power 132 (2) (2010).